

Crystallization kinetics and corrosion behaviors of $Mg_{61}Cu_{28}Gd_{11}$ and $(Mg_{0.61}Cu_{0.28}Gd_{0.11})_{99.5}Sb_{0.5}$ amorphous alloys

SUN Ying-di, LI Zi-quan, LIU Jin-song, YANG Ji-nian, CONG Meng-qi

College of Materials Science and Technology, Nanjing University of Aeronautics and Astronautics,
Nanjing 210016, China

Received 17 June 2010; accepted 15 August 2010

Abstract: 0.5% (molar fraction) Sb was added to $Mg_{61}Cu_{28}Gd_{11}$ glass forming alloy to improve its thermal stability and corrosion resistance. The crystallization kinetics of $Mg_{61}Cu_{28}Gd_{11}$ and $(Mg_{0.61}Cu_{0.28}Gd_{0.11})_{99.5}Sb_{0.5}$ amorphous alloys was investigated under continuous heating. The temperatures of glass transition, onset and peak crystallization for the two glasses exhibit strong heating-rate dependence. The activation energies for the onset and peak crystallization were determined based on the Ozawa plots. Vogel-Fulcher-Tamman equation analysis shows that the larger strength parameter and much longer relaxation time are obtained due to the Sb addition. The corrosion properties of the two glassy alloys were studied by means of potentiodynamic and immersion tests. Compared with the parent alloy, $(Mg_{0.61}Cu_{0.28}Gd_{0.11})_{99.5}Sb_{0.5}$ glassy alloy exhibits a superior corrosion resistance in Cl^- -containing alkaline solution, as indicated by the lower passive current density and corrosion rate. Based on the point defect model, the effect mechanism of Sb addition on corrosion resistance of Mg-Cu-Gd glassy alloy is carefully identified.

Key words: Mg-based bulk metallic glasses; Sb; crystallization kinetics; corrosion resistance

1 Introduction

Mg-based bulk metallic glasses (BMGs) have attracted increasing interest during the last decade due to their high specific strength and relatively low cost. Among them, Mg-TM-RE (TM: transition metal; RE: rare-earth metal, such as Y and Gd) alloy system has been known to exhibit a large supercooled liquid region (SLR) and high glass-forming ability (GFA)[1–4]. Ever since the first search that discovered $Mg_{65}Cu_{25}Y_{10}$ BMG with a size of 4 mm in diameter, a great deal of effort has been devoted to develop Mg-based BMGs[5–8]. Recently, ZHENG et al[9] reported that the best ternary Mg-based glassy former has been found in the composition of $Mg_{61}Cu_{28}Gd_{11}$ with the maximum size up to 12 mm in diameter. The follow-up investigations on the Mg-Cu-Gd-based BMGs have been directed to the addition of a proper element to improve its GFA and other properties, such as Mg-Cu-B-Gd, Mg-Cu-Gd-Be, Mg-Cu-Ag-Gd-Ni, Mg-Cu-Gd-Nb and Mg-Cu-Ag-Gd[10–15]. In particular, the addition of silver seems to result in the best GFA, and the critical diameter of $Mg_{54}Cu_{26.5}Ag_{8.5}Gd_{0.11}$ glassy alloys has achieved 25 mm

by a Cu-mold injection casting method[15]. As promising engineering materials, the thermal stability (i.e. crystallization resistance) and corrosion resistance of Mg-based BMGs are usually considered the important aspects for their application, and thus have received great attention in recent years.

To date, the addition of quaternary element is an effective method to improve the crystallization resistance of Mg-Cu-RE (RE=Y, Gd) glassy alloy. CHENG et al[16] have studied the effect of B addition on crystallization kinetics of $Mg_{65}Cu_{25}Y_{10}$ glassy alloy, and confirmed that the minor B element appears to enhance the thermal stability of Mg-Cu-Y-B alloy. CHANG et al[17] have investigated the crystallization processes of $Mg_{65}Cu_{25}Gd_{10}$ glassy alloy with Ag addition. It has been found that the activation energy of crystallization is increased by minor addition of Ag, and the main crystallization process for $Mg_{65}Cu_{22.5}Gd_{10}Ag_{2.5}$ glassy alloy is governed by diffusion controlled crystal growth with decreasing nucleation rate[17]. As can be seen, both B and Ag elements have negative heat of mixing (ΔH_m) with the main constituents of Mg-Cu-Y/Gd glassy alloys[18]. However, Sb element which exhibits partial positive ΔH_m with main constituents has not been

previously reported to improve the thermal stability of Mg-Cu-Gd glassy alloy.

In addition, corrosion behavior of Mg-Cu-RE (RE=Y, Gd) BMGs has been also investigated in recent years. QIN et al[19] conducted corrosion tests of $\text{Mg}_{65}\text{Cu}_{25}\text{Gd}_{10}$ in 0.2 mol/L $\text{H}_3\text{BO}_3/\text{Na}_2\text{B}_4\text{O}_7$ (pH=8.4), 0.02 mol/L NaCl (pH=11) and 0.1 mol/L NaOH (pH=13) solutions, and found that $\text{Mg}_{65}\text{Cu}_{25}\text{Gd}_{10}$ BMGs showed higher corrosion resistance than its crystalline counterpart. Moreover, in Cl^- -containing alkaline solution, both amorphous and crystalline $\text{Mg}_{65}\text{Cu}_{25}\text{Gd}_{10}$ alloys are active dissolved at high current density due to the presence of aggressive Cl^- ion in the solution[19]. Similar results have also been found in Mg-Cu-Y glassy alloys[20–21]. To date, there is still lack of study for the improvement of corrosion resistance by microalloying technique in Mg-Cu-Gd alloy system within Cl^- -containing alkaline solution.

This work aims to investigate the crystallization and corrosion behaviors of $\text{Mg}_{61}\text{Cu}_{28}\text{Gd}_{11}$ and $(\text{Mg}_{0.61}\text{Cu}_{0.28}\text{Gd}_{0.11})_{99.5}\text{Sb}_{0.5}$ BMGs and explore the effect mechanism of minor addition of Sb on thermal stability and corrosion resistance of Mg-Cu-Gd glassy alloy by the differential scanning calorimetry (DSC) technique and electrochemical measurements.

2 Experimental

Elements with purity better than 99.9% were used as starting materials. Since the boiling points of Mg and Sb are lower than those of Cu and Gd, Cu-Gd as intermediate alloy was melted prior to be re-melted with Mg and Sb in an arc furnace under an argon atmosphere. The glasses were prepared by copper mold casting with a diameter of 2 mm and a length of 50 mm.

The structures of the samples obtained were examined by X-ray diffractometer (XRD, Bruker D8) with Cu K_α radiation. The crystallization process of the $\text{Mg}_{61}\text{Cu}_{28}\text{Gd}_{11}$ and $(\text{Mg}_{0.61}\text{Cu}_{0.28}\text{Gd}_{0.11})_{99.5}\text{Sb}_{0.5}$ amorphous alloys were characterized by continuous heating in a DSC (Perkin-Elmer DSC 7) under flowing high purity argon. A set of DSC scans was recorded at heating rates ranging from 10 to 80 K/min. The corrosion behavior was evaluated by electrochemical measurements. The electrolyte used was 0.01 mol/L NaCl solution with pH 12 (adjusted by 1 mol/L NaOH). Electrochemical measurements were conducted in a three-electrode cell using a platinum counter electrode and a saturated calomel reference electrode (SCE). Potentiodynamic polarization curves were measured with a potential sweep rate of 1 mV/s in the solution open to air at room temperature after immersing the specimens for about 20 min. Electrochemical impedance spectroscopy (EIS) was also measured at open-circuit

potential in the solution. The frequency range used was from 10^5 to 10^{-2} Hz, with an amplitude perturbation of 5 mV. The mass loss measurements of the glassy alloys were conducted in 0.01 mol/L NaCl alkaline solution after immersing for 100 h. Corrosion effects on the surface topography of immersed specimens were studied by scanning electron microscopy (SEM).

3 Results and discussion

3.1 Microstructures

Fig.1 shows the XRD patterns of as-prepared $\text{Mg}_{61}\text{Cu}_{28}\text{Gd}_{11}$ and $(\text{Mg}_{0.61}\text{Cu}_{0.28}\text{Gd}_{0.11})_{99.5}\text{Sb}_{0.5}$ glassy alloys. The diffraction patterns consist only of broad diffraction peaks in the 2θ range of 32° – 42° , indicating the formation of a single glassy phase.

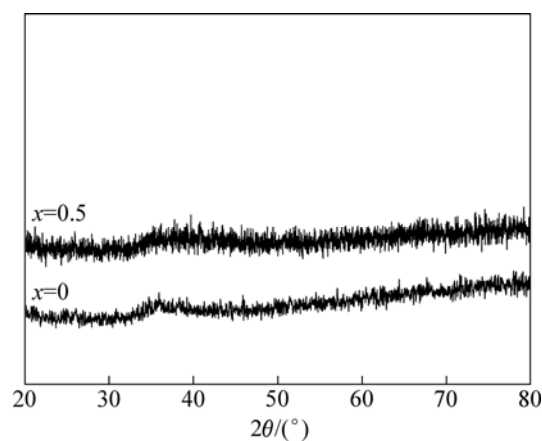


Fig.1 XRD patterns of as-prepared $(\text{Mg}_{0.61}\text{Cu}_{0.28}\text{Gd}_{0.11})_{100-x}\text{Sb}_x$ ($x=0, 0.5$) BMGs

3.2 Crystallization kinetics

Fig.2 shows the DSC curves for $\text{Mg}_{61}\text{Cu}_{28}\text{Gd}_{11}$ and $(\text{Mg}_{0.61}\text{Cu}_{0.28}\text{Gd}_{0.11})_{99.5}\text{Sb}_{0.5}$ glassy alloys obtained at various heating rates of 10, 20, 30, 40 and 80 K/min. The values of glass transition temperature T_g , onset temperature of crystallization T_x , peak temperature T_p and ΔT_x (defined as temperature region between T_g and T_x) shift to higher temperatures with increasing the heating rate, as shown in Fig.3. The crystallization of samples is rate dependent caused by the fact that nucleation is a thermally activated process, whereas the rate dependence of the kinetic glass transition is due to the relaxation processes in the glass transition region[22]. The effective activation energy of crystallization processes can be calculated by means of the Ozawa equation[23–24]:

$$\ln \phi = -1.0516 \frac{E}{RT} + \text{constant} \quad (1)$$

where ϕ is the heating rate; R is the molar gas constant; T represents the thermodynamically characteristic

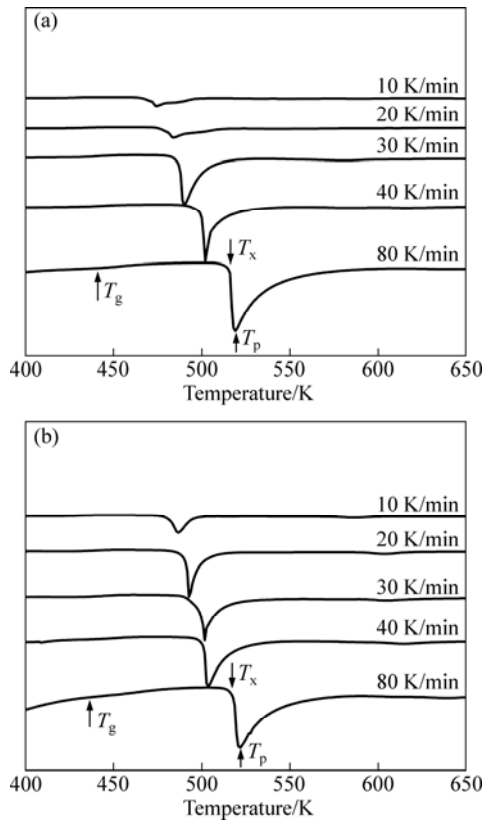


Fig.2 Continuous heating DSC curves of $\text{Mg}_{61}\text{Cu}_{28}\text{Gd}_{11}$ (a) and $(\text{Mg}_{0.61}\text{Cu}_{0.28}\text{Gd}_{0.11})_{99.5}\text{Sb}_{0.5}$ (b) amorphous alloys at different heating rates of 10, 20, 30, 40 and 80 K/min

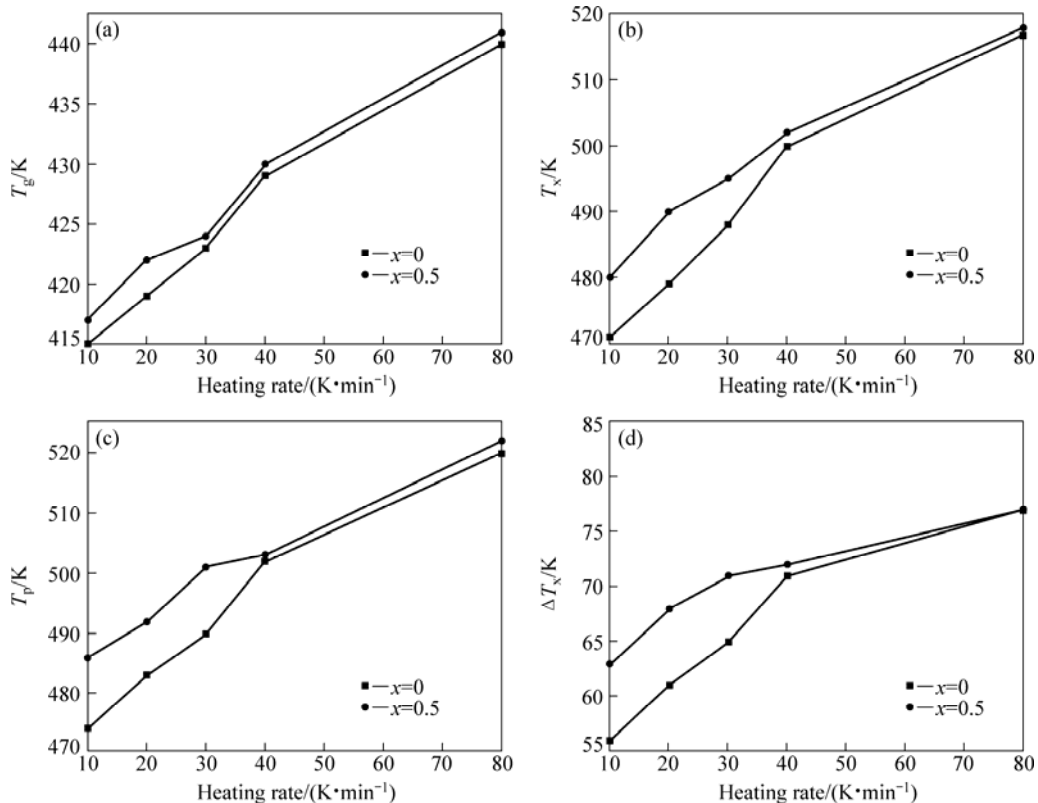


Fig.3 Variation of characteristic temperatures T_g (a), T_x (b), T_p (c) and ΔT_x (d) of $(\text{Mg}_{0.61}\text{Cu}_{0.28}\text{Gd}_{0.11})_{100-x}\text{Sb}_x$ ($x=0, 0.5$) glassy alloys at different heating rates

temperature, such as T_x or T_p . The plots of $\ln\phi$ against $1/T$ yield an approximate straight line with a slope of E_x and E_p , as shown in Fig.4, in which E_x is the effective activation energy for the onset temperature of crystallization, and E_p is the effective activation energy for the peak temperature. Thus, we obtained $E_x=81$ kJ/mol, $E_p=89$ kJ/mol for $\text{Mg}_{61}\text{Cu}_{28}\text{Gd}_{11}$ glassy alloy, and $E_x=106$ kJ/mol, $E_p=111$ kJ/mol for $(\text{Mg}_{0.61}\text{Cu}_{0.28}\text{Gd}_{0.11})_{99.5}\text{Sb}_{0.5}$ glassy alloy. E_x and E_p of Sb-containing alloy are about 31% and 25% higher, respectively, than those of the parent alloy, suggesting the improvement of crystallization resistance in $(\text{Mg}_{0.61}\text{Cu}_{0.28}\text{Gd}_{0.11})_{99.5}\text{Sb}_{0.5}$ glassy alloy.

The dependence of the glass transition temperature T_g on the heating rate ϕ could be evaluated in terms of Vogel-Fulcher-Tamman (VFT) equation written in the form [25]:

$$\phi = B \exp \left[\frac{DT_g^0}{T_g^0 - T_g} \right] \quad (2)$$

where T_g^0 is the asymptotic value of onset glass transition T_g when the cooling or heating rate is infinitely slow; B is the relaxation time dimension under the ideal state; and D is the strength parameter. Based on Eq.(2), we obtained three adjustable parameters: B , D , and T_g^0 , as listed in Table 1. Fig.5 shows the best VFT fitting curves of the two glassy alloys. As can be seen, B and D parameters of Sb-containing alloy are both considerably

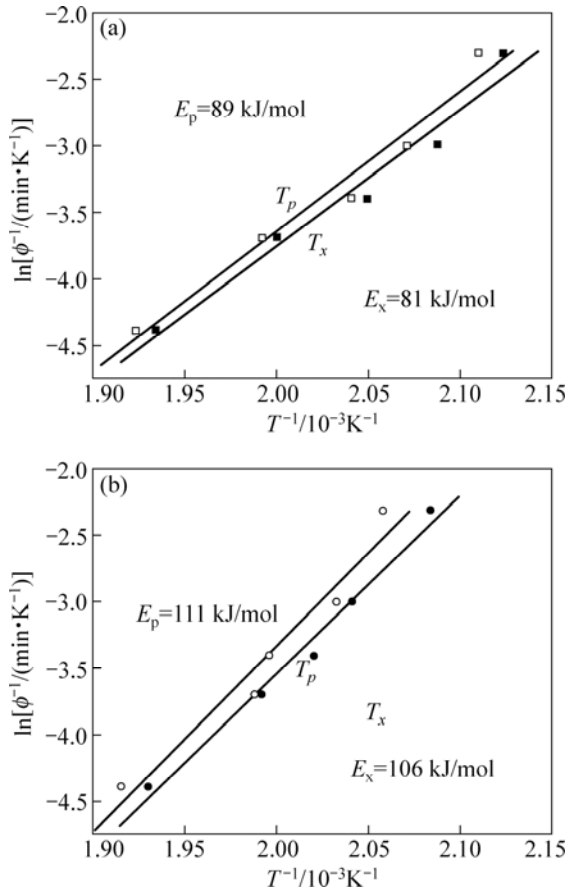


Fig.4 Ozawa plots of T_x and T_p for $Mg_{61}Cu_{28}Gd_{11}$ (a) and $(Mg_{0.61}Cu_{0.28}Gd_{0.11})_{99.5}Sb_{0.5}$ (b) amorphous alloys

Table 1 VFT fitting results of $Mg_{61}Cu_{28}Gd_{11}$ and $(Mg_{0.61}Cu_{0.28}Gd_{0.11})_{99.5}Sb_{0.5}$ glassy alloys

Sample	T_g^0/K	$B/(K \cdot s^{-1})$	D
$Mg_{61}Cu_{28}Gd_{11}$	397.8	293.2	0.15
$(Mg_{0.61}Cu_{0.28}Gd_{0.11})_{99.5}Sb_{0.5}$	389.1	1 006.8	0.31

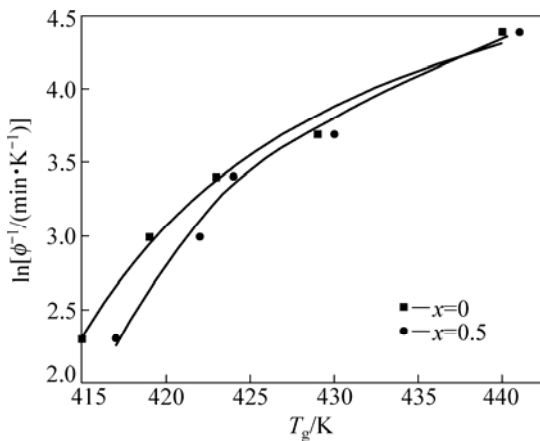


Fig.5 VFT fitting curves of as-prepared $(Mg_{0.61}Cu_{0.28}Gd_{0.11})_{100-x}Sb_x$ ($x = 0, 0.5$) BMGs

larger than those of the parent alloy while the value of T_g^0 is slightly smaller, indicating the increase of strength and relaxation time in $(Mg_{0.61}Cu_{0.28}Gd_{0.11})_{99.5}Sb_{0.5}$ glassy alloy.

The local activation energy $E_c(x)$ usually indicates the potential barrier that is overcome during the transformation of amorphous to crystallized phase. Its variation with crystallized fraction (x) reflects the nucleation and growth behavior in the crystallization process. In order to calculate local activation energy, crystallized fraction x as functions of temperature T at different heating rates for $Mg_{61}Cu_{28}Gd_{11}$ and $(Mg_{0.61}Cu_{0.28}Gd_{0.11})_{99.5}Sb_{0.5}$ glassy alloy are plotted in Figs.6(a) and (b), respectively. From the following equation, suggested by Ozawa-Flynn-Wall for non-isothermal crystallization, the local activation energy for crystallization $E_c(x)$ can be evaluated [26]:

$$\ln \phi = -1.0516 \frac{E_c(x)}{RT(x)} + \text{constant} \quad (3)$$

where $E_c(x)$ is local activation energy and $T(x)$ is the temperature corresponding to the certain crystallized volume fraction, x , at different heating rates. From Eq.(3), for a given x , T values of different heating rates are determined. $E_c(x)$ can be calculated by the slope of $\ln \phi$ against $1/T_x$ curve. Fig.6(c) shows the plots of $E_c(x)$ as a function of x for the two glassy alloys. Note that, $Mg_{61}Cu_{28}Gd_{11}$ and $(Mg_{0.61}Cu_{0.28}Gd_{0.11})_{99.5}Sb_{0.5}$ alloys exhibit the similar tendency of the variation of $E_c(x)$ with increasing x . At the beginning, the values of $E_c(x)$ are 81 kJ/mol and 106 kJ/mol, respectively for $Mg_{61}Cu_{28}Gd_{11}$ and $(Mg_{0.61}Cu_{0.28}Gd_{0.11})_{99.5}Sb_{0.5}$ glassy alloys. Subsequently, $E_c(x)$ values increase slowly with x during the very initial crystallization stage and reach the maximum values at $x=0.2$, to be 103 kJ/mol and 131 kJ/mol, respectively, for the above alloys. Then, $E_c(x)$ values decrease drastically in the subsequent crystallization process and remain 60 kJ/mol and 67 kJ/mol at $x=0.95$, respectively, for the parent and Sb-containing alloys. The variation of $E_c(x)$ with x can be attributed to the nucleation and growth behaviors at different stage of crystallization process. In the early stage of crystallization, the nucleation and growth of micro-grains need to overcome larger potential barrier, which would further increase with the increase in temperature. However, when the crystallized volume fraction achieves a certain point at $x=0.2$, the potential barrier would not increase due to the structural relaxation of amorphous phases surrounding the crystal phases. On the other hand, the Sb-containing alloy exhibits higher $E_c(x)$ value during the whole crystallization process, indicating that the crystallization resistance as well as thermal stabilities is improved by minor addition of Sb. This is in consistent with the result of Ozawa methods. The better thermal stability obtained by Sb-containing

glassy alloy could be attributed to multiple factors. The larger overall atomic size difference (the atomic size ratios: 0.899 for Sb/Mg, 0.889 for Cu/Sb and 0.809 for Sb/Gd) and higher overall electronegativity difference would induce the increment of packing density of $(\text{Mg}_{0.61}\text{Cu}_{0.28}\text{Gd}_{0.11})_{99.5}\text{Sb}_{0.5}$ alloy in supercooled liquid. In addition, the strong affinity for Sb/Mg ($\Delta H_m = -16$ kJ/mol) and Sb/Gd ($\Delta H_m = -68$ kJ/mol)[18], together with the weak repellency for Sb/Cu ($\Delta H_m = 7$ kJ/mol) will even impose resistance to the formation of the major Mg_2Cu phase, possibly by blocking the path of Mg and Cu

diffusion. Thus, the crystallization energy barrier would be increased indirectly, which could result in the final improvement of crystallization resistance in Sb-containing glassy alloy.

3.3 Electrochemical results

Fig.7(a) shows the polarization curves of $(\text{Mg}_{0.61}\text{Cu}_{0.28}\text{Gd}_{0.11})_{100-x}\text{Sb}_x$ ($x=0, 0.5$) glassy alloys in 0.01 mol/L NaCl solution with pH 12. The corrosion data, including the corrosion potential (ϕ_{corr}), current density (J_{corr}), the passive potential (E_p) and passive current density (J_p) are summarized in Table 2. It can be seen that the parent and Sb-containing alloys both exhibit a high corrosion potential and low corrosion current density, implying the excellent corrosion resistance of Mg-Cu-Gd glassy materials. In addition, the minor addition of Sb element results in a positive and significant shift of the corrosion potential by about 277 mV. The corrosion current density of the Sb-containing alloy ($0.130 \mu\text{A}/\text{cm}^2$) is even lower than that of the parent alloy ($32.3 \mu\text{A}/\text{cm}^2$). Furthermore, as compared with the parent alloy, the Sb-containing alloy exhibits a better passivation in 0.01 mol/L NaCl alkaline solution

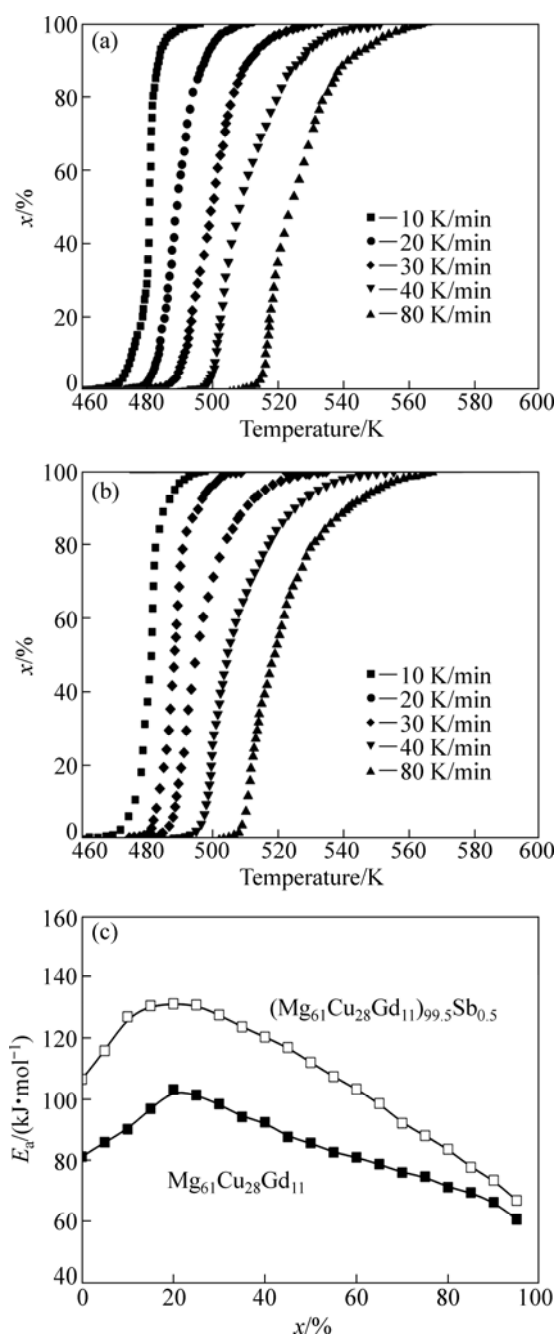


Fig.6 Crystallized volume fraction x as function of temperature for $\text{Mg}_{61}\text{Cu}_{28}\text{Gd}_{11}$ (a) and $(\text{Mg}_{0.61}\text{Cu}_{0.28}\text{Gd}_{0.11})_{99.5}\text{Sb}_{0.5}$ (b) glassy alloys at different heating rates, and variation of activation energy during crystallization process (c)

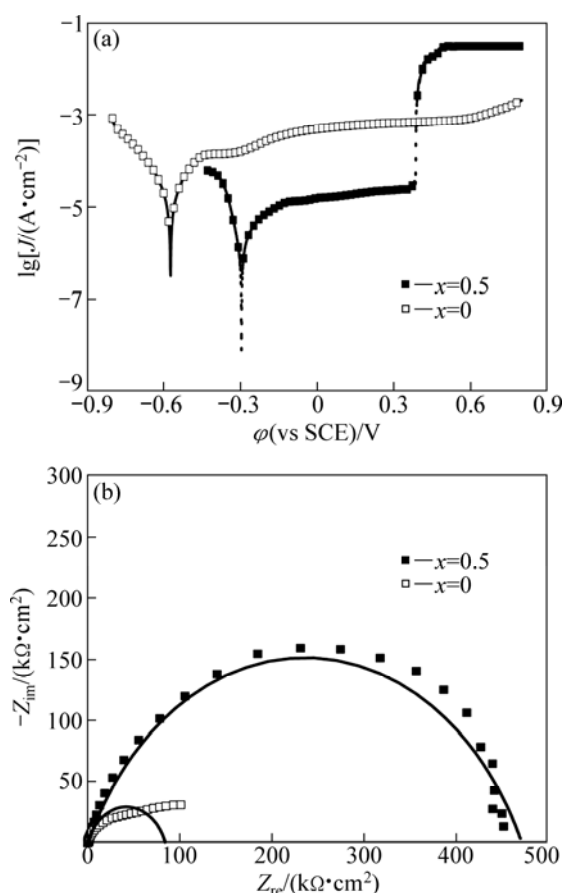


Fig.7 Polarization curves of $(\text{Mg}_{0.61}\text{Cu}_{0.28}\text{Gd}_{0.11})_{100-x}\text{Sb}_x$ ($x=0, 0.5$) BMGs in 0.01 mol/L NaCl alkaline solutions (pH 12) at open-circuit potential (a), and their corresponding Nyquist diagrams (b)

Table 2 Corrosion data obtained from potentiodynamic polarization curves and immersion test in 0.01 mol/L NaCl alkaline solutions (pH 12) at open-circuit potential for two glassy alloys

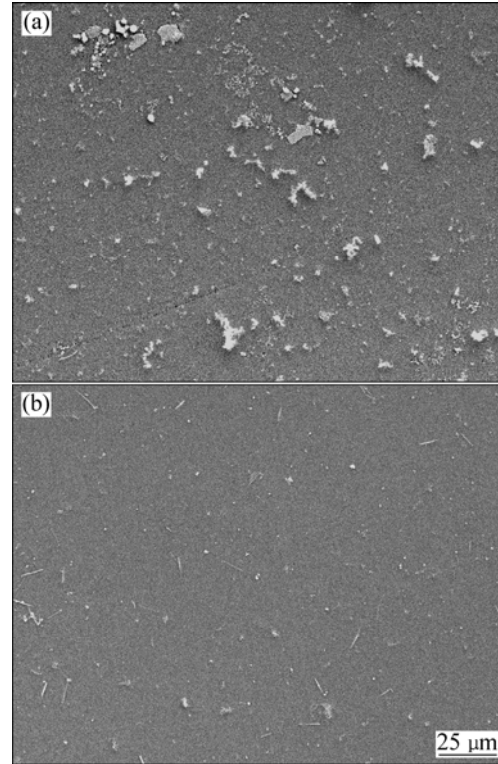
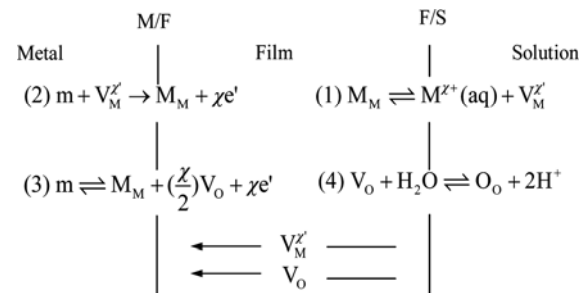
Sample	$\varphi_{\text{corr}}/\text{mV}$	$J_{\text{corr}}/(\mu\text{A}\cdot\text{cm}^{-2})$	$J_{\text{p}}/(\mu\text{A}\cdot\text{cm}^{-2})$	E_{p}/mV	$R_{\text{corr}}/(\text{mm}\cdot\text{a}^{-1})$
Mg ₆₁ Cu ₂₈ Gd ₁₁	-573.4	32.3	138.1	-492.3	0.119
(Mg _{0.61} Cu _{0.28} Gd _{0.11}) _{99.5} Sb _{0.5}	-296.1	0.1	11.4	-188.4	0.049

with extremely lower passive current density (11.4 $\mu\text{A}/\text{cm}^2$), which is about a tenth of that of the parent alloy. However, when the anodic voltage increases to 0.386 V, the corrosion current density of Sb-containing alloy abruptly increases to the order of 10^{-2} A/cm² due to the breakdown of the passive film.

From Fig.7(b), it can be noticed that EIS of both Mg₆₁Cu₂₈Gd₁₁ and (Mg_{0.61}Cu_{0.28}Gd_{0.11})_{99.5}Sb_{0.5} glassy alloys in Cl⁻-containing alkaline solution show only one capacitive loop, meaning that the corresponding electrode process contains only one time constant and the minor addition of Sb does not change the corrosion mechanism of the parent alloy. In addition, the single capacitive loop also indicates the formation of uniform passive films in the two glassy alloys. On the other hand, the larger impedance of (Mg_{0.61}Cu_{0.28}Gd_{0.11})_{99.5}Sb_{0.5} glassy alloy implies that the introduction of Sb in Mg-Cu-Gd glassy alloy increases its polarization resistance and further decreases the electrochemical charge of interfacial reaction. This is in good agreement with the potentiodynamic polarization result in Fig.7(a).

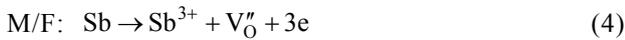
The corrosion rates of the two glassy alloys could be calculated from the mass loss measurement in 0.01 mol/L NaCl alkaline solution at 298 K, as listed in Table 2. The Sb-containing alloy exhibits much lower corrosion rate (0.049 mm/a) than the parent alloy (0.119 mm/a). The SEM micrographs of the two glassy alloys after immersing in 0.01 mol/L NaCl alkaline solution for 100 h are shown in Fig.8. Compared with Mg₆₁Cu₂₈Gd₁₁ glassy alloy, the surface morphology of the Sb-containing alloy is much more homogeneous and smooth, no obvious pitting attacks occur. The better corrosion resistance of (Mg_{0.61}Cu_{0.28}Gd_{0.11})_{99.5}Sb_{0.5} glassy alloy can be attributed to the higher standard electrode potentials (-0.66 V) of Sb addition in alkaline solution compared with Mg and Gd. This would result in a nobler state of the Sb-containing glassy alloy and thus increase the corrosion resistance of Mg-Cu-Gd BMGs.

Based on the “point defect model, PDM” theory[27], the corrosion mechanism of Sb-containing alloy can be further explained. Fig.9 shows the physico-chemical processes that occur within a passive film according to the PDM theory[27–28]. During the growth of passive film, cation vacancies V_{M}^{\prime} are first formed at the film/solution (F/S) interface, but then will be consumed at the metal/film (M/F) interface, while the anion vacancies V_{O}^- are on the opposite. The oxygen-ions from the F/S will diffuse continuously into M/F and

**Fig.8** Surface SEM micrographs of Mg₆₁Cu₂₈Gd₁₁ (a) and (Mg_{0.61}Cu_{0.28}Gd_{0.11})_{99.5}Sb_{0.5} (b) metallic glasses after immersion in 0.01 mol/L NaCl alkaline solutions with pH=12 for 100 h**Fig.9** Schematic diagram of physico-chemical processes occurring within passive film according to point defect model[27] (m =metal atom, M_{M} =metal cation in cation site, $M_{\text{M}}^{\chi+}(\text{aq})$ =hydro-metal, O_{O} =oxygen ion anion site, V_{M}^{\prime} =cation vacancy, V_{O}^- =anion vacancy)

result in the initial growth of passive film. Thus, at the beginning of anodic reaction in the Cl⁻-containing alkaline solution, the Sb element can be presumed to be Sb³⁺ cations at the M/F interface, and then are oxidized to be Sb⁵⁺ cations at the F/S interface. Subsequently, the

cations will be separated from the outer layer of passive film and enter into the alkaline solution. This would result in the formation of high valence vacancies in the described as follows:



It should be noticed that the formation of oxygen-ions in Procedure (4) of Fig.9 is only suitable for the neutral and acidic solution. For the Cl^- -containing alkaline solution, Procedure (4) could be described as follows:



The diffusion of oxygen-ions is performed through the above electrochemical reactions (4)–(7). Based on the ion mobility equation proposed by FROMHOLD and COOK[29] and high-field approximation, the concentration of oxygen-ions $c'_\text{O}(x)$ can be determined as the following formulas:

$$c'_\text{O}(x) = k_2 \left[\left(k_4^{-1} - \frac{n}{2} \frac{a}{D'_\text{O}} \right) \exp(-x/a) + \frac{n}{2} \frac{a}{D'_\text{O}} \right] \quad (8)$$

$$D'_\text{O} = \frac{D_\text{O}}{2} \exp[2FaE/(RT)] \quad (9)$$

where D_O is the diffusion coefficient of oxygen-ions in the passive film; E is electric field strength; a is ionic jump distance ($a \approx 3 \times 10^{-8}$ cm); F is Faraday constant; R is molar gas constant; T is temperature; $k_i (i=1, 2, 3, 4)$ is reaction rate constant. For the Sb-containing glassy alloy, the modified formula of oxygen-ions concentration can be determined as follows:

$$c'_\text{O}(x) = (k_2 + k_{2,\text{Sb}}) \left[\left(k_4^{-1} - \frac{n}{2} \frac{a}{D'_\text{O}} \right) \exp(-x/a) + \frac{n}{2} \frac{a}{D'_\text{O}} \right] \quad (10)$$

By comparing Eqs.(8) with (10), the oxygen-ions concentration is increased apparently by the introduction of Sb. This may further accelerate the formation of oxides at the M/F interface, and then improve the growth of passive film.

4 Conclusions

1) The crystallization kinetics analysis shows that E_x and E_p of Sb-containing alloy are about 31% and 25% higher, respectively, than those of the parent alloy. The dependence of the glass transition on the heating rate was analyzed in terms of the VFT equation, and the superior strength parameter D and much longer relaxation time B were obtained for $(\text{Mg}_{0.61}\text{Cu}_{0.28}\text{Gd}_{0.11})_{99.5}\text{Sb}_{0.5}$ glassy

alloy.

2) $\text{Mg}_{61}\text{Cu}_{28}\text{Gd}_{11}$ and $(\text{Mg}_{0.61}\text{Cu}_{0.28}\text{Gd}_{0.11})_{99.5}\text{Sb}_{0.5}$ alloys exhibit the similar tendency of the variation of local activation energy $E_c(x)$ with increasing the crystallized volume fraction x . The Sb-containing alloy exhibits higher $E_c(x)$ during the whole crystallization process, indicating that the crystallization resistance as well as thermal stabilities is improved by minor addition of Sb.

3) The results of potentiodynamic and immersion tests reveal that the minor addition of Sb could considerably enhance the corrosion resistance of the parent alloy in the Cl^- -containing alkaline solutions, as indicated by the lower corrosion current density, $\sim 0.130 \mu\text{A}/\text{cm}^2$, and depressed corrosion rate, $\sim 0.049 \text{ mm/a}$. Based on the PDM theory, the increase of oxygen-ions concentration at the M/F interface of Sb-containing alloy would accelerate the growth of passive film.

References

- [1] INOUE A, MASUMOTO T. Production and properties of light-metal-based amorphous alloys [J]. *Materials Science and Engineering A*, 1991, 133: 6–9.
- [2] SOUBEYROUX J L, PUECH S, BLANDIN J J. Synthesis of new Mg-based bulk metallic glasses with high glass forming ability [J]. *Materials Science and Engineering A*, 2007, 449–451: 253–256.
- [3] GOLDEN K, TANG H X, SCHROERS J. Nanomoulding with amorphous metals [J]. *Nature*, 2009, 457: 868–872.
- [4] HUANG J C, CHU J P, JANG J S C. Recent progress in metallic glasses in Taiwan [J]. *Intermetallics*, 2009, 17(12): 973–987.
- [5] JANG J S C, TSENG C T, YEH Y C, JOU J L, HUANG J C. Thermoplastic forming properties and microreplication ability of a magnesium-based bulk metallic glass [J]. *Advanced Engineering Materials*, 2008, 10(11): 1048–1052.
- [6] CHEN H M, LEE C J, HUANG J C, LI T H, JANG J S C. Flow serration and shear-band propagation in porous Mo particles reinforced Mg-based bulk metallic glass composites [J]. *Intermetallics*, 2010, 18(6): 1240–1243.
- [7] KINAKA M, KATO H, HASEGAWA M, INOUE A. High specific strength Mg-based bulk metallic glass matrix composite highly ductilized by Ti dispersoid [J]. *Materials Science and Engineering A*, 2008, 494(1–2): 299–303.
- [8] JANG J S C, JIAN S R, LI T H, HUANG J C, TSAO C A, LIU C T. Structural and mechanical characterizations of ductile Fe particles-reinforced Mg-based bulk metallic glass composites [J]. *Journal of Alloys and Compounds*, 2009, 485(1–2): 290–294.
- [9] ZHENG Q, CHENG S, XU J, MA H, XU J. Critical size and strength of the best bulk metallic glass former in the Mg-Cu-Gd ternary system [J]. *Scripta Materialia*, 2007, 56: 161–164.
- [10] CHANG Y C, HUANG J C, CHENG Y T, LEE C J, DU X H, NIEH T G. On the fragility and thermomechanical properties of Mg-Cu-Gd(B) bulk metallic glasses [J]. *Journal of Applied Physics*, 2008, 103(10): 103521–1–6.
- [11] LI Z G, HUI X, ZHANG C M, WANG M L, CHEN G L. Strengthening and toughening of Mg-Cu-(Y, Gd) bulk metallic glasses by minor addition of Be [J]. *Materials Letters*, 2007, 61(28): 5018–5021.
- [12] PAN D G, LIU W Y, ZHANG H F. Mg-Cu-Ag-Gd-Ni bulk metallic glass with high mechanical strength [J]. *Journal of Alloys and*

- Compounds, 2007, 438(1–2): 142–144.
- [13] ZHANG C M, HUI X, LI Z G, CHEN G L. Improving the strength and the toughness of Mg-Cu-(Y, Gd) bulk metallic glass by minor addition of Nb [J]. Journal of Alloys and Compounds, 2009, 467(1–2): 241–245.
- [14] CHANG Y C, HUANG J C, CHENG Y T, LEE C J, DU X H, NIEH T G. Effect of silver or boron on viscosity and thermomechanical properties in Mg-Cu-Gd metallic glasses [J]. Journal of Applied Physics, 2008, 103(10): 103521.
- [15] MA H, SHI LL, XU J, LI Y, MA E. Discovering inch-diameter metallic glasses in three-dimensional composition space [J]. Applied Physics Letters, 2005, 87: 181915.
- [16] CHENG Y T, HUNG T H, HUANG J C, HSIEH P J, JANG J S C. Thermal stability and crystallization kinetics of Mg-Cu-Y-B quaternary alloys [J]. Materials Science Engineering A, 2007, 449–451: 501–505.
- [17] CHANG L J, JANG J S C, YANG B C, HUANG J C. Crystallization and thermal stability of the $Mg_{65}Cu_{25-x}Gd_{10}Ag_x$ ($x=0-10$) amorphous alloys [J]. Journal Alloys and Compounds, 2007, 434–435: 221–224.
- [18] TAKEUCHI A, INOUE A. Classification of bulk metallic glasses by atomic size difference, heat of mixing and period of constituent elements and its application to characterization of the main alloying element [J]. Materials Transactions JIM, 2005, 46: 2817–2829.
- [19] QIN F X, BAE G T, DAN Z H, LEE H, KIM N J. Corrosion behavior of the $Mg_{65}Cu_{25}Gd_{10}$ bulk amorphous alloys [J]. Materials Science Engineering A, 2007, 449–451: 636–639.
- [20] GEBERT A, WOLFF U, JOHN A, ECKERT J. Corrosion behavior of $Mg_{65}Y_{10}Cu_{25}$ metallic glass [J]. Scripta Materialia, 2000, 43: 279–283.
- [21] YAO H B, LI Y, WEE A T S. Corrosion behavior of melt-spun $Mg_{65}Ni_{20}Nd_{15}$ and $Mg_{65}Cu_{25}Y_{10}$ metallic glasses [J]. Electrochimica Acta, 2003, 48: 2641–2650.
- [22] BUSHCH R, KIM Y J, JOHNSON W L. Thermodynamics and kinetics of the undercooled liquid and the glass transition of the $Zr_{41.2}Ti_{13.8}Cu_{12.5}Ni_{10.0}Be_{22.5}$ alloy [J]. Journal of Applied Physics, 1995, 77: 4039–4043.
- [23] OZAWA T. Kinetics of glass crystallization [J]. Journal of Thermal Analysis and Calorimetry, 1970, 15: 301–305.
- [24] OZAWA T. Kinetics of non-isothermal crystallization [J]. Polymer, 1971, 12: 150–158.
- [25] BRÜNING R, SAMWER K. Glass transition on long time scales [J]. Physical Review B, 1992, 46: 11318–11322.
- [26] FLYNN J H. The isoconversional method for determination of energy of activation at constant heating rates [J]. Journal of Thermal Analysis and Calorimetry, 1983, 27: 95–102.
- [27] URQUIDI-MACDONALD M, MACDONALD D D. Theoretical distribution functions for the breakdown of passive films [J]. Journal of Electrochemical Society, 1987, 134: 41–43.
- [28] LIU B, LIU L, CHEN Z Y. Effect of micro Mo addition on anticorrosion ability of Cu base bulk metallic glass [J]. Acta Metallurgica Sinica, 2007, 43: 82–86.
- [29] FROMHOLD A T J, COOK E L. Diffusion currents in large electric fields for discrete lattices [J]. Journal of Applied Physics, 1967, 38: 1546–1553.

Mg₆₁Cu₂₈Gd₁₁ 和 (Mg_{0.61}Cu_{0.28}Gd_{0.11})_{99.5}Sb_{0.5} 非晶合金的 晶化动力学和腐蚀行为

孙颖迪, 李子全, 刘劲松, 杨继年, 丛孟启

南京航空航天大学 材料科学与技术学院, 南京 210016

摘要: 研究 0.5%(摩尔分数)Sb 的引入对 Mg₆₁Cu₂₈Gd₁₁ 块体非晶合金性能的影响。利用差热扫描量热仪测试样品的晶化动力学。结果表明: 在等时加热的过程中, 非晶合金的玻璃转变温度、起始晶化和峰值晶化温度都表现出对加热速率强的依赖性。基于 Oawza 方法可以确定非晶合金的起始晶化和峰值晶化激活能。Vogel-Fulcher-Tamman 公式分析表明: 含 Sb 元素的非晶合金具有更高的强度系数和更长的延迟时间。采用电化学极化和失重测试方法研究 2 种玻璃合金的腐蚀行为。与基体非晶合金相比, 添加微量 Sb 降低了非晶合金的在含 Cl⁻ 的碱性溶液中的钝化电流密度和腐蚀速率, 表现出相比基体合金更为优越的耐蚀性。最后基于“点缺陷模型”进一步分析微量 Sb 元素对基体合金耐蚀性能的影响机理。

关键词: Mg 基大块金属玻璃; Sb; 晶化动力学; 耐蚀性

(Edited by YANG Hua)